EMCH 402

Experimental Stress Analysis

Technical Report for Laboratory Exercise 1

Stress and Strain Analysis of Materials using Strain Gages

Author (Lead Author): *Eden, Jake*

Sections Authored*: Cover Page, Introduction, and Theory*

Co-author: *Sipos, Emre*

Sections Authored*: Methods and Materials and Applications*

Co-author: *Gupta, Ankit*

Sections Authored*: Results and Discussion and Conclusion*

Writing Team Number: *5*

Tuesday 12:00-1:00pm

Submission Date: *18 March 2024*

Introduction:

Engineers are constantly looking for ways to increase response to stress and strain and maximize material properties. One possible method to increase the response to stress and strain is through changing the orientation of the fibers in the material. This lab's objective is to test and evaluate if the orientation of fibers can have a statistically significant impact on how a material responds to stress and strain. Understanding what can impact intended responses from stress and strain is critical for success in the engineering world.

To accomplish the objective of this lab, the group used two carbon epoxy specimens. One specimen had layers that alternated with an orientation of [0°/90°], while the second specimen had layers that alternated with orientation of [-45°/+45°]. Both specimens were of similar dimensions to explore how orientation of fibers can impact the response to stress. The hypothesis is that each of the specimen will exhibit differing responses to stress and strain due to fundamental differences in laminae orientation Furthermore, these fundamental orientation differences are expected to yield higher stress and strain responses for the alternating layers of [-45°/+45°].

During this lab's experimental testing phase, the specimens were placed into an MTS Qtest ball screw electro-mechanical testing machine with strain gages attached directly to the specimens in the axial and transverse directions. The MTS Qtest ball screw electro-mechanical testing machine will apply an increasing stress load to the specimen in the axial direction to create a strain in the specimen being tested. A true understanding of the testing technique is critical to ensure that the proper data is collected. For example, the data being collected in this lab is a voltage output that can be converted into a stress to create a stress-strain curve for the two specimens. To successfully collect this data, the proper machine needed to be used, which is why proper understanding of the testing equipment is critical for every experiment. Using the MTS Qtest ball screw electro-mechanical testing machine in this lab helps broaden the horizons of possible testing techniques to collect proper data for analysis.

While the testing technique is an important step of the experiment, the data collection and analysis portion are just as critical. Data was collected in this lab by attaching the strain gages to a Wheatstone Bridge to measure a change in resistance to record a voltage output. This voltage output was then converted to a stress value using governing equations for sensitivity, Wheatstone bridge conversions, and Hooke's law. Material properties were then able to be calculated from the stress value and analysis can be conducted to explore differences between the two specimens.

Theory:

To perform the lab properly and accurately it is critical that the theory being studied is understood. The theory needs to be properly applied in a lab setting to gain intended results. For example, all materials will react differently under stress, so understanding why is crucial to understand what exactly is being tested. On top of this, other topics are impacted by theory as well such as the selection of the proper strain gage.

Material Theory

As previously discussed, the material specimen for this lab is made from a carbon/epoxy laminate. These specimens are considered composites, and composites have specific traits that impact their response to stress. Composites are made of two materials. The first is the matrix, which gives the composite its

lightweight properties, while the second is the reinforcements [1]. The matrix holds reinforcement in its orderly pattern as well as helping to transfer the load along the reinforcement. Each composite was formed with layers of an alternating direction of fibers. The reinforcements help give the lamina its strength and stiffness properties. The reinforcements are either particulates or fibers. This lab used fibers, which are most common and allow for high axial strength [1]. In a theoretical environment, discontinuous fibers, which were used in this lab, are stronger than particulates but weaker than continuous fibers that are used in high performance scenarios. The discontinuous fibers add extra strength without excessive price increases that continuous fibers can bring. The combination of these factors is what gives the lamina its strength, but other factors such as the direction of fibers also have a significant impact.

The structure of this lamia is a bidirectional lamina. This means that the fibers run in two different directions to create a woven pattern. Figure 1 shows how the θ alternates between layers of specimen 1. Figure 2 shows how the orientation will be laid out for specimen 2. For specimen two, the layers will alternate between a positive and negative of this θ.

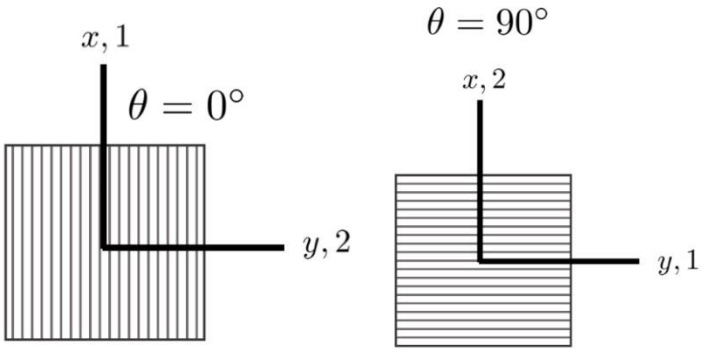

Figure 1. The figure above shows the orientation of fibers in layers of specimen 1.

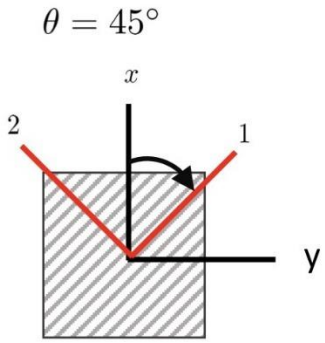

Figure 2. The figure above shows the orientation of fibers in specimen 2.

The bidirectional fibers create an anisotropic material. An anisotropic material has varying mechanical properties and strength depending on the direction it is being measured from. This is where the transversely isotropic theory is applied. The transversely isotropic theory defines material properties, such as elasticity and strength, in different directions within the material. To apply this theory, one plane must have the same properties in all directions. Due to this, it is assumed that the transverse plane, the y-z plane due to the load being applied in x direction, will have the same properties in all directions due to

symmetry. The elastic constants are isotropic in this plane, which means that the number of independent constants can be reduced. Due to this theory, the following simplifications can be made:

$$E_y = E_z$$

$$\upsilon_{xy} = \upsilon_{xz}$$

$$\upsilon_{yz} = \upsilon_{zy}$$

$$G_{xy} = G_{xz}$$

Figure 3 shows the typical stress-strain matrix. The simplifications above can reduce the number of unknown constants from nine to six. To dive into more theory on this topic, plane stress is also able to reduce the number of unknown constants [1]. For example, plane stress in this lab, due to the direction of the force applied, has plane stress in the Y-Z plane. This means that G_{yz} and υ_{yz} equal zero. This leaves only 4 unknown elastic constants. As these constants, such as σ_{xx}, the other unknown unknown constants can be solved for, which gives values to important properties such as strain, elastic modulus, and shear modulus. The simplifications from the transverse isotropic theory are what make it possible to solve for these constants.

$$\begin{Bmatrix} \varepsilon_{xx} \\ \varepsilon_{yy} \\ \varepsilon_{zz} \\ \gamma_{xy} \\ \gamma_{yz} \\ \gamma_{xz} \end{Bmatrix} = \begin{bmatrix} \frac{1}{E_x} & -\frac{\upsilon_{yx}}{E_y} & -\frac{\upsilon_{zx}}{E_y} & 0 & 0 & 0 \\ -\frac{\upsilon_{xy}}{E_x} & \frac{1}{E_y} & -\frac{\upsilon_{yz}}{E_y} & 0 & 0 & 0 \\ -\frac{\upsilon_{xy}}{E_x} & -\frac{\upsilon_{yz}}{E_y} & \frac{1}{E_y} & 0 & 0 & 0 \\ 0 & 0 & 0 & \frac{1}{G_{xy}} & 0 & 0 \\ 0 & 0 & 0 & 0 & \frac{1}{G_{yz}} & 0 \\ 0 & 0 & 0 & 0 & 0 & \frac{1}{G_{xy}} \end{bmatrix} \begin{Bmatrix} \sigma_{xx} \\ \sigma_{yy} \\ \sigma_{zz} \\ \tau_{xy} \\ \tau_{yz} \\ \tau_{xz} \end{Bmatrix}$$

Figure 3. The figure above shows a matrix relating strain and stress through various material constants.

Strain Gage Theory

Attached to the material being tested was a strain gage, which has its own theory behind the selection of the proper gage. The three main components of strain gage selection are sensitivity, temperature compensation, and gage factor. The change of resistance of the strain gage and its relationship to the applied strain of the test specimen is strain gage sensitivity [2]. The resistance of the conductor, or the wire, can be represented from the equation:

$$R = \rho * \frac{L}{A} \qquad (1)$$

In the equation above, ρ is the resistivity, L is length, and A is area. These values give a value for resistance. Through taking the natural log of the equation, followed by a differential, and then applying the log-derivative method, the following equation is formed:

$$\frac{\frac{dR}{R}}{\varepsilon_a} = 1 + 2\upsilon + \frac{\frac{d\rho}{\rho}}{\varepsilon_a} \tag{2}$$

The equation is theoretically significant because sensitivity, which will be denoted using S_a, is related to the equation by the relationship shown below in equation 3. To expand on this, that relationship can be substituted into equation 4, also shown below, to develop an equation for sensitivity. In equation 4, 2υ refers to the dimensional change of the conductor, while $\frac{\frac{d\rho}{\rho}}{\varepsilon_a}$ refers to the change in specific resistance [2].

$$S_a = \frac{\frac{dR}{R}}{\varepsilon_a} \tag{3}$$

$$S_a = 1 + 2\upsilon + \frac{\frac{d\rho}{\rho}}{\varepsilon_a} \tag{4}$$

Closely related to sensitivity is the gage factor. The gage factor is the ratio of change in resistance to mechanical strain [3]. The gage factor equation is shown below in equation five, and equation 6 shows the gage factor relationship to sensitivity.

$$GF = \frac{\frac{\Delta R}{R}}{\varepsilon_a} \tag{5}$$

$$\frac{\frac{dR}{R}}{\varepsilon_a} \approx \frac{\frac{\Delta R}{R}}{\varepsilon_a} \tag{6}$$

The significance of these two properties is that in experimental applications specific sensitivity levels are desirable to ensure that accurate strain data will be collected. Furthermore, sensitivity at a higher level can increase accuracy and resolution in the collection of data. Due to this theory, an additional strain gage was added positioned in the transverse direction to increase overall sensitivity. Since there are sensitivities in the transverse (S_t) direction as well, another relationship is formed to account. This relationship is shown below in equation 7. The third component of that relationship, shear sensitivity (S_s), is ignored due to the assumption that shear strains are small compared to the axial and transverse directions [3]. Moreover, by defining a transverse sensitivity factor, K_t, the equation can be simplified more into what is shown in equation 9. This final relationship is the governing response of a bonded strain gage.

$$\frac{\Delta R}{R} = S_a\varepsilon_a + S_t\varepsilon_t + S_s\gamma_{at} \tag{7}$$

$$K_t = \frac{S_t}{S_a} \tag{8}$$

$$\frac{\Delta R}{R} = S_a(\varepsilon_a + K_t\varepsilon_t) \tag{9}$$

While accuracy and gage factor can have an impact in accuracy of data, it also is crucial in calibration. For commercial strain gages, there is a manufacturer's gage factor, which is denoted as S_g. The equation

for gage factor is shown below in equation 10. In experimental applications, a strain gage would be bent on a beam to a specific strain in the axial direction (ε_a) [3]. Once this occurs, ΔR is measured and S_g can be calculated from equation 10. Equation 12 below relates S_g to S_a and K_t. The constant in the equation, v_0, is calculated using equation 11, but this value is typically accepted to be 0.285.

$$\frac{\Delta R}{R} = S_g \varepsilon_a \tag{10}$$

$$v_0 = -\frac{\varepsilon_t}{\varepsilon_a} \tag{11}$$

$$S_g = S_a(1 - v_0 K_t) \tag{12}$$

Transverse sensitivity can also cause error, which needs to be calculated to find the actual strain that will be used to calculate the stress-strain response. This is done by substituting equation 12 into equation 9 and simplifying. This process simplifies down into equation 13 below. The actual strain is denoted using ε_{act}. In the equation below, $\frac{\frac{\Delta R}{R}}{S_g}$ can be substituted for the apparent strain (ε'_a). To put this into a practical application, ε_{act} can also be denoted as ε_{xx}, ε_t can be denoted by ε_{yy}, and ε'_a can be denoted as ε'_{xx} as shown in the relations below. These relations can be substituted into equation 12 to create a practical equation as seen in equation 14. This is how errors will be corrected in the axial (x) direction.

$$\varepsilon_{act} = \varepsilon'_a \frac{1 - v_0 K_t}{1 + K_t \frac{\varepsilon_t}{\varepsilon_{act}}} \tag{13}$$

$$\varepsilon_{act} \equiv \varepsilon_{xx}$$

$$\varepsilon_t \equiv \varepsilon_{yy}$$

$$\varepsilon'_a \equiv \varepsilon'_{xx}$$

$$\varepsilon_{xx} = \varepsilon'_{xx} \frac{1 - v_0 K_t}{1 + K_t \frac{\varepsilon_{yy}}{\varepsilon_{xx}}} \tag{14}$$

Error also occurs in the transverse (y) direction, so new relationships are formed as seen below to form equation 15.

$$\varepsilon_{act} \equiv \varepsilon_{yy}$$

$$\varepsilon_t \equiv \varepsilon_{xx}$$

$$\varepsilon'_a \equiv \varepsilon'_{yy}$$

$$\varepsilon_{yy} = \varepsilon'_{yy} \frac{1 - v_0 K_t}{1 + K_t \frac{\varepsilon_{xx}}{\varepsilon_{yy}}} \tag{15}$$

The final component to the theory of strain gage selection is temperature compensation. Just like mechanical stresses, apparent strain can be induced thermally due to temperature change [3]. The coefficient of thermal expansion should match between the material and strain gage to ensure there is similar thermal expansion. If one were to expand more than the other, there would be errors in the data

collected as the strain gage could acquire inaccurate strain data. The temperature induced change in gage resistance, denoted as $(\frac{\Delta R}{R})_{\Delta T}$, has three contributing factors [3]. The first, shown in equation 16, is the grid elongation of the strain gage. The known variables in this equation can be used to find the coefficient of thermal expansion (CTE), which is represented by α. The specimen elongation, b in equation 17, also contributes to the overall gage resistance. The last contributing factor is the temperature coefficient of resistivity, which is γ in equation 18. All three of these constants come together in equation 19 to create a relationship for the change in resistance due to thermal expansion.

$$\frac{\Delta L_{grid}}{L_{grid}} = \alpha \Delta T \tag{16}$$

$$\frac{\Delta L_{specimen}}{L_{specimen}} = b \Delta T \tag{17}$$

$$\frac{\Delta R_{gage}}{R} = \gamma \Delta T \tag{18}$$

$$(\frac{\Delta R}{R})_{\Delta T} = S_g(b - \alpha)\Delta T + \gamma \Delta T \tag{19}$$

Wheatstone Bridge Theory

The $\frac{\Delta R}{R}$ data being collected needs to be converted to a Δv_0. To accomplish this, a Wheatstone bridge is used. The Wheatstone bridge is comprised of four resistors connected at four points that will be represented by A, B, C, and D as seen in Figure 4 below. Resistors 1 and 2 are the voltage dividers on the top leg, while resistors three and four divide the bottom leg [4]. Equations 20 and 21 show the voltage division of the two legs in the Wheatstone bridge. The equation includes the voltage from the voltage source which is denoted by v_s. Furthermore, since the change in output voltage is used to determine strain, it is important to understand how it is calculated. Equation 22 shows how the output voltage is calculated using internal voltages from the Wheatstone bridge, while equation 23 substitutes the resistors and voltage source into the equation. While this gives an overall output voltage, it is not the change in output voltage that is desired for the testing in the lab. Equation 24 below is used to find the change in output voltage. Equation 25 simplifies the previous equation by expanding and neglecting higher order terms. This theory is critical to understand because resistance levels would need to be adjusted to achieve a desired output voltage in some cases. Having four resistors that do not work together would yield inaccurate results, so understanding how everything must work together allows for accurate results to be collected.

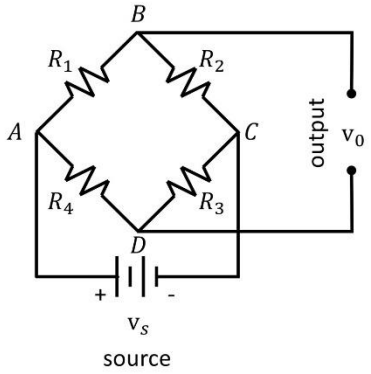

Figure 4. The diagram above shows the construction of a Wheatstone bridge.

$$V_{AB} = \frac{R_1}{R_1+R_2} v_s \quad (20)$$

$$V_{AD} = \frac{R_4}{R_3+R_4} v_s \quad (21)$$

$$v_0 = V_{AB} - V_{AD} \quad (22)$$

$$v_0 = \frac{R_1R_3-R_2R_4}{(R_1+R_2)(R_3+R_4)} v_s \quad (23)$$

$$\Delta v_0 = \frac{(R_1+\Delta R_1)(R_3+\Delta R_3)-(R_2+\Delta R_2)(R_4+\Delta R_4)}{(R_1+\Delta R_1+R_2+\Delta R_2)(R_3+\Delta R_3+R_4+\Delta R_4)} v_s \quad (24)$$

$$\Delta v_0 = \frac{R_1R_2}{(R_1+R_2)^2}\left(\frac{\Delta R_1}{R_1} - \frac{\Delta R_2}{R_2} + \frac{\Delta R_3}{R_3} - \frac{\Delta R_4}{R_4}\right) v_s \quad (25)$$

Similarly to strain gages, sensitivity is also a important factor in Wheatstone bridges. The relationship of sensitivity to strain changes depending on the type of voltage applied [4]. This lab tests a variable voltage, to increase strain and find failure. In the governing equations below, R_g=R_1. Also, sensitivity will be denoted using S_c, gage current will be denoted with I_g, and the power dissipated by the gage will be represented by P_g. Equation 26 below relates the source voltage to the gage current and resistance. Equation 27 forms a relationship for current and resistance for the power dissipated by the gage in order to perform a substitution that forms equation 28. This final equation relates the circuit sensitivity to the gage sensitivity, power dissipated by the gage, as well as the resistance. This shows that sensitivity depends on gage selection as well as the relationship of $r = \frac{r}{(r+1)}$, where $r = \frac{R_2}{R_g}$ [4].

$$v_s = I_g R_g (1 + r) \quad (26)$$

$$I_g R_g = \sqrt{P_g R_g} \quad (27)$$

$$S_c = \frac{r}{(1+r)} S_g \sqrt{P_g R_g} \quad (28)$$

There is theory behind all aspects of this lab and ensuring that the theory comes together and is applied properly to yield the desired results. The theory also explains choices such as material selections which will be elaborated in this next section of this report.

Materials and Methods:

Composite Materials

The composite samples studied in this exercise were comprised of carbon/epoxy laminates oriented at either [0°/90°], or [+45°/-45°]. In these composites, laminates were stacked on top of each other at alternating bi-directional cross-ply orientations (i.e. 45/-45/-45/45 or 0/90/90/0) as seen in figure 5 [1].

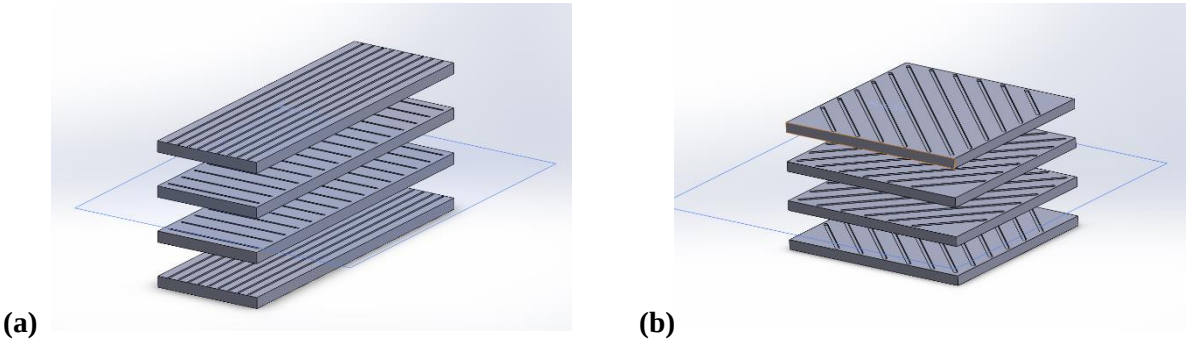

(a) **(b)**

Figure 5. 3-D model of bi-directional orientations: (a) [0°/90°] alternating laminate orientations; and (b) [+45°/-45°] alternating laminate orientations [5].

The process used to stack and manufacture these varied orientation samples is known as Vacuum Assisted Resin Transfer Molding or VARTM for short. In this process, a mold was first prepared for each unique fiber orientation. Next, the mold was sealed in a vacuum-tight environment where resin is drawn through the mold by the vacuum as seen in figure 6. Once the resin has coated the entirety of the mold, it was left to cure at which point another layer of different orientation was added until desired material thickness was achieved [6].

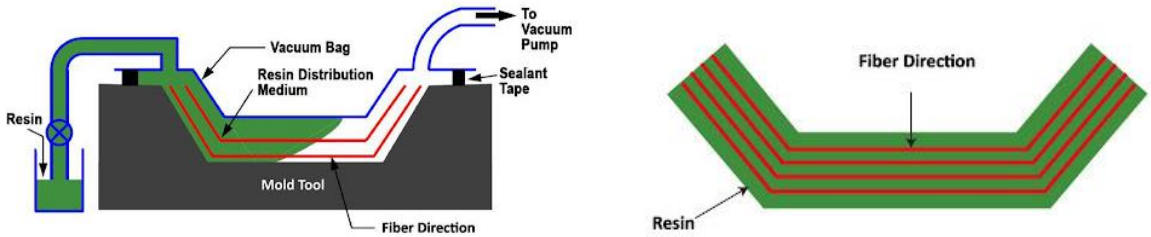

Figure 6. VARTM Fabrication Process Diagram: Illustrating the impact of mold tool, vacuum pump, and fiber direction on manufacturing of composites [6].

The first bi-directional (cross-ply) orientation of [0°/90°] consisted of four alternating woven layers presenting a cloth-like woven appearance. However, it is important to note that the pattern was symmetrical about the midplane of the layers. This means that the layer orientation above and below the midplane will be a mirror reflection. Expanding the [0°/90°] orientation to long-hand (0/90/0/90/90/0/90/0) and revisiting figure 5 provides a better visual understanding of this concept. Similarly, the second bi-directional cross-ply orientation of [+45°/-45°] consisted of the same layering techniques, but due to the orientation presenting a smooth and homogeneous appearance. The [+45°/-45°] sample was also symmetrical about the midplane of its layers [5].

Strain Gages Selection

The strain gage selected for this experiment was coded with designation CEA-00-375UW-120. The “CE” designation referred to the carrier matrix which is thin and flexible featuring copper coated soldering tabs for direct lead wire attachment that enabled a sound connection to the Wheatstone bridge. The “A” designation referred to the foil alloy which was a constantan alloy featured. The “00” designation referred to the self-temperature compensation which was in self-temperature compensated form. The “375” designation referred to the active gage length in increments of 0.001 inches meaning the selected gage was 9.525 mm. The “UW” designation referred to the grid and tab geometry which represented the U-wire grid pattern and weldable tabs. The most important designation was the “120” which referred to the resistance in ohms of the gage. This was important because it indicated compatibility for the Wheatstone bridge and Vishay Model 2100 Amplifier. Finally, due to the nature of the experiment, considerations for test duration and cyclic endurance were not large factors. It was known prior to the experiment that specimen were to be tested to failure meaning that single use and easy installment with correct resistance compatibility had significant impact on the selection of the CEA-00-375UW-120 in particular [7]. Further information on strain gage specifications can be found in figure 18 in the appendix.

Strain Gages Installment

For each of the carbon/epoxy laminates, two strain gages were prepared and secured to the gaging area with one being in the longitudinal and the other being in the transverse direction of the specimen as seen in figure 7. The process of securing the gages to the specimen was meticulous and involved an in-depth surface preparation to ensure a clean installment. The workbench and specimen were first cleaned with Acetone to remove any large imperfections. Following this the surface was abraded with M-Prep Conditioner A (figure 19a), 150 rough grit sandpaper, and 400 grit fine sandpaper. The final preparatory step before gage transfer was to neutralize the surface with M-Prep Neutralizer 5A (figure 19b) and let the surface area dry [5].

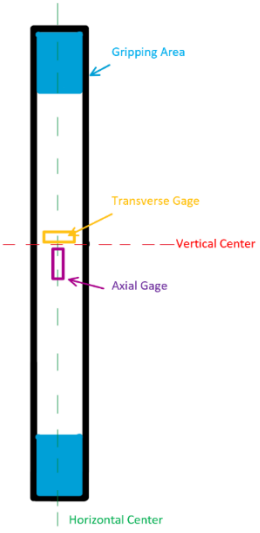

Figure 7. Strain Gage Preparation Schematic: Visually explains the optimal placement of transverse and axial gages as well as the anticipated gripping area for MTS Qtest ball screw electro-mechanical testing machine jaws.

Gage transfer began with carefully marking vertical and horizontal center lines within the gaging area seen in figure 7. Following this precise mark, a gage was removed from packaging and placed onto a piece of tape to allow easier repositioning. After the gage was lined up with tape, a thin layer of catalyst was applied and allowed to dry. Immediately after drying, adhesive was layered onto the catalyst and the gage was pressed down onto the specimen having pressure applied for over a minute. Carefully pulling back the tape from the corner of the gage at a high angle yielded a well bonded gage on each of our specimen as seen in figure 20 of the appendix. Following this strong adhesion, lead wires were carefully soldered onto the soldering tabs and the resistance was checked on a multimeter which read roughly 120 Ω [5].

The critical nature of ensuring a clean bond between specimen and gage lied within the distinct advantages of a strain gage over other tensile testing methods. More specifically, strain gages were not directly subjected to external loads, enabling them to provide more precise measurements on impact of forces acting within an object. Furthermore, these more precise measurements are obtained wherever a strain gage can be secured cleanly to a material. This matters in our experiment due to the fabrication imperfections of our specimen that were observed in initial material acquisition. Our specimen had different dimensions for width and thickness at different intervals of length. While the differences are marginal, when exposing the specimen to extreme forces like the MTS Qtest ball screw electro-mechanical testing machine is capable of, these slight imperfections would have had larger experimental impacts had strain gages not been used.

Tensile Testing

The machine used for testing the specimen in this lab was the MTS Qtest ball screw-electro-mechanical testing machine with an incremental tensile capacity of 22,500 lbs (about 10206 kg). The specimen was first loaded into the wedge grips and tightened down with the machine contacting the specimen in the gripping area as seen in figure 8.

Figure 8. Loaded Specimen in MTS Qtest ball screw electro-mechanical testing machine jaws: Jaws are secured on specimen no more than 2” down the gripping area at even heights.

Before tensile testing could be completed, gain adjustment needed to be completed for the 0-10 volt range of the amplifier for both load and strain ranges. Based on the given gage factor of 2.115 and a theoretical gage factor of 2 conversions could be derived for anticipated experimental outcomes and are found in tables 1 and 2. The purpose of adjusting for the maximum amount of anticipated micro-strain the sample will experience was to increase the resolution of data acquisition. Using known outcomes of previous experiments, the amount of micro-strain per volt was reduced which increased the number of pixels on the x-axis of the data acquisition software when data was observed [8].

Table 1. Conversion Factors for [0°/90°] sample:

Load	1V = 2250 lbs
Transverse	1V = 500 με
Longitudinal	1V = 2000 με

Table 2. Conversion Factors for [+45°/-45°] sample:

Load	1V = 2250 lbs
Transverse	1V = 12048.19 με
Longitudinal	1V = 12048.19 με

Additionally, the balancing of the Wheatstone bridge needed to be completed prior to tensile testing, which utilized previously calculated correction factors and fine adjustments on the amplifier driven by internal shunt resistors. First, the red lead wire was connected to p+ terminal row on the peg in the fifth column of the Wheatstone bridge. Next the white lead wire was attached to the s- terminal row on the peg in the fifth column of the Wheatstone bridge. Finally, the black lead wire was attached to the D120 terminal row on the peg in the fifth column of the Wheatstone bridge [8]. This lead wire connection configuration can be seen in figure 9.

Figure 9. Lead Wire Connection Configuration on Wheatstone Bridge: White lead wire is connected to the s- terminal, black lead wire connected to the D120 terminal, and red lead wire is connected to the p+ terminal.

The built in ballast resistors allowed modifications of outbound voltage yielding the specific conversion factors discussed in the tables above. This process was done on the Model 2100 Vishay amp with the two LED system which can be seen in figure 10.

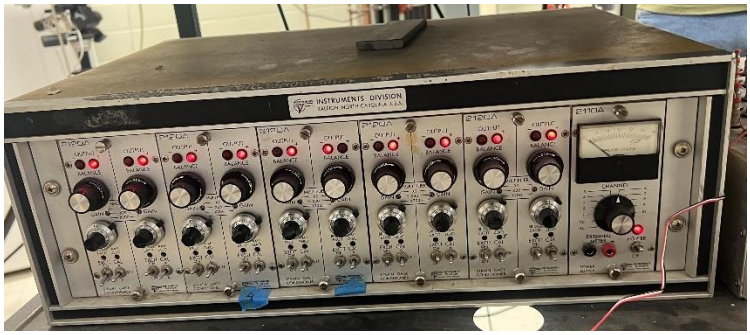

Figure 10. Model 2100 Vishay Amplifier Configuration: Shows the two light interface that is utilized to balance the Wheatstone bridge as well as the gain knob which gain adjustments are used to make.

Incrementally adjusting the balance knob until both output lights on the amp were dim indicated a balanced bridge that was ready for testing. Following the balance of the Wheatstone bridge with the specimen secured data collection began on the accompanied desktop data acquisition software. The displacement rates for experimental testing of each specimen can be seen below in table 3. The reason for the discrepancies in displacement rates was for the sake of time. It is known that the [+45°/-45°] sample can sustain a higher load than the [0°/90°] sample meaning a higher displacement rate was necessary to save time while simultaneously retaining sensitivity.

Table 3. Displacement rates for each specimen:

[0°/90°] sample	0.05 inches/minute

[+45°/-45°] sample	0.15 inches/minute

Results and Discussion:

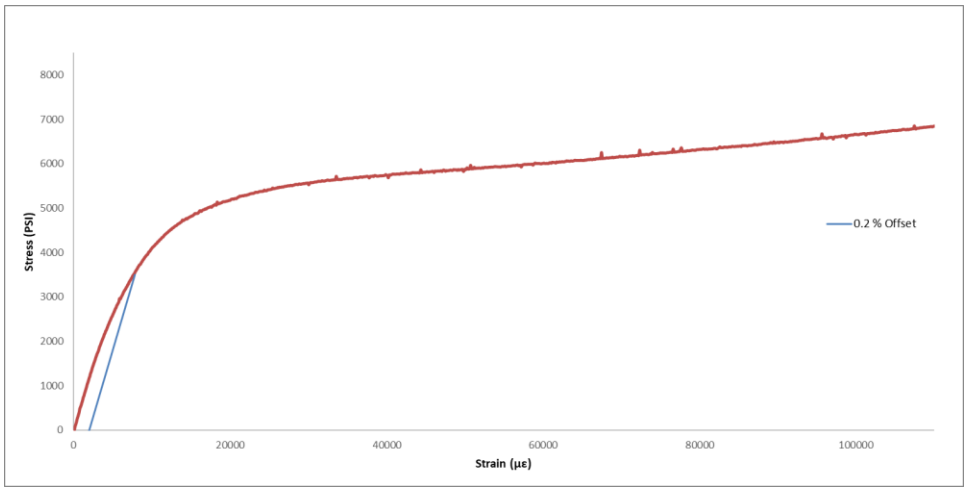

Figure 11. Plot of Shear Stress vs Shear Strain for determining the max Shear Stress and the Offset Shear Strength

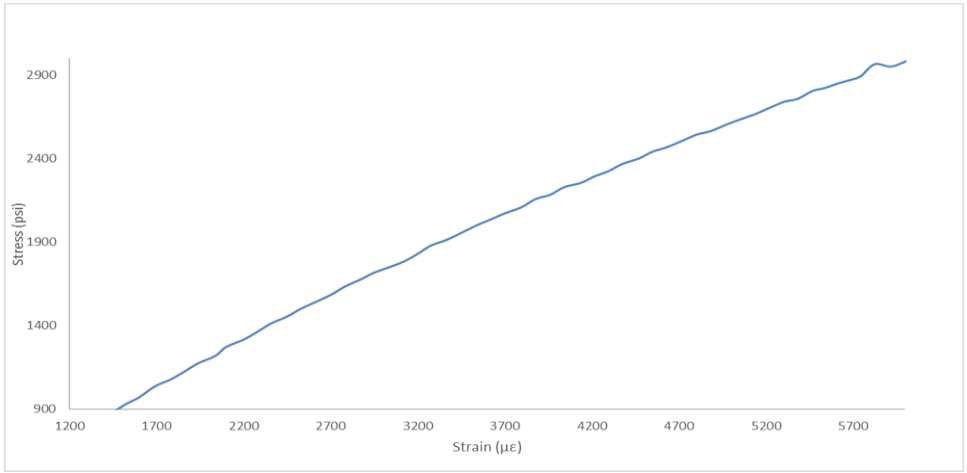

Figure 12. Plot of Shear Stress vs Shear Strain zoom in on the Chord Shear Modulus Measurement

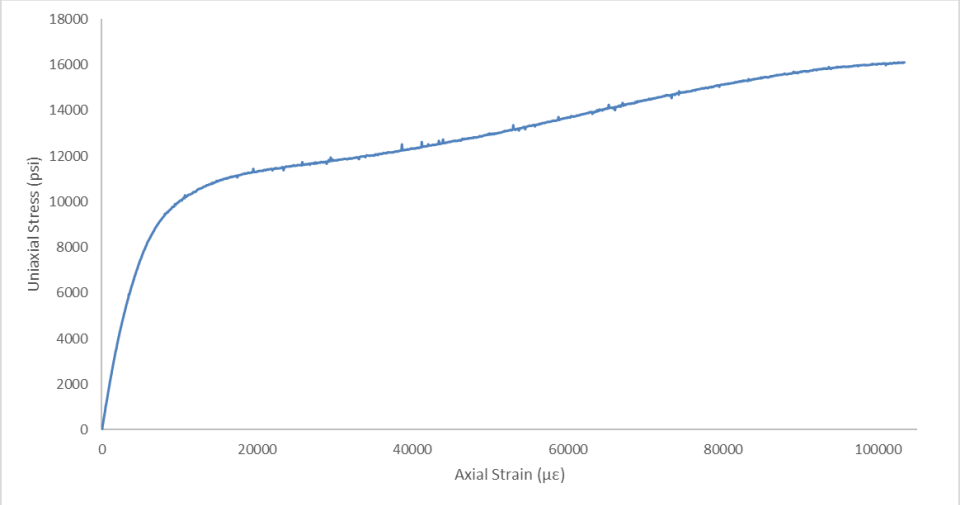

Figure 13. Plot of Uniaxial Stress vs Axial Strain to determine the Laminate Failure Strength

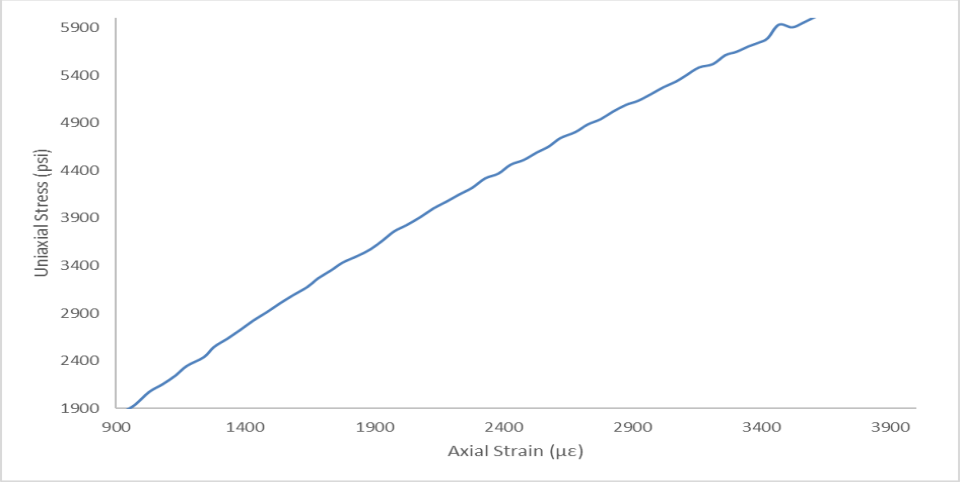

Figure 14. Plot of Uniaxial Stress vs Axial Strain zoom in on the Chord Modulus Measurement

In analyzing the material properties influenced by fiber orientation, the [+45°/-45°] orientation revealed both elastic and plastic behaviors. By employing the chord method outlined in the ASTM D3518/D3518M standards, refer Appendix, we derived significant insights from the data depicted in Figures 11 through 14. Based on Table 4, the shear modulus (G_{12}), using chord method, was determined to be 0.462 MSI. This calculation, alongside observations of a maximum load of 1645 lb and a peak shear stress of 5.884 ksi, shows the impact of fiber orientation on material performance. Furthermore, the recorded ultimate tensile strength stood at 16.127 ksi, accompanied by an Elastic Modulus (E) of 1.6 MSI, calculated using chord method. Particularly, Figure 11 highlights the 0.2% Offset Shear Strength, which was derived from the shear stress and strain data, illustrating the enhanced shear strength attributable to the [+45°/-45°] fiber arrangement. These results support the hypothesis that fiber orientation significantly influences a material's response to stress and strain, demonstrating the exceptional shear strength achieved by the [+45°/-45°] orientation.

Table 4. In-plane shear material properties using [+45°/-45°]$_s$ per ASTM standard D 3518/D 3518M.						
Modulus, G_{12} (by chord method)	Maximum Load P^m	Maximum Shear Stress,	Offset Shear Strength, F_{12}(o.2% offset)	Maximum Shear Strain	Modulus, E (by chord method)	Ultimate Tensile Strength, F^{tu}
0.462 MSI	1645 lb	5.884 ksi	3500 psi	0.05 in/in	1.6 MSI	16.127 ksi

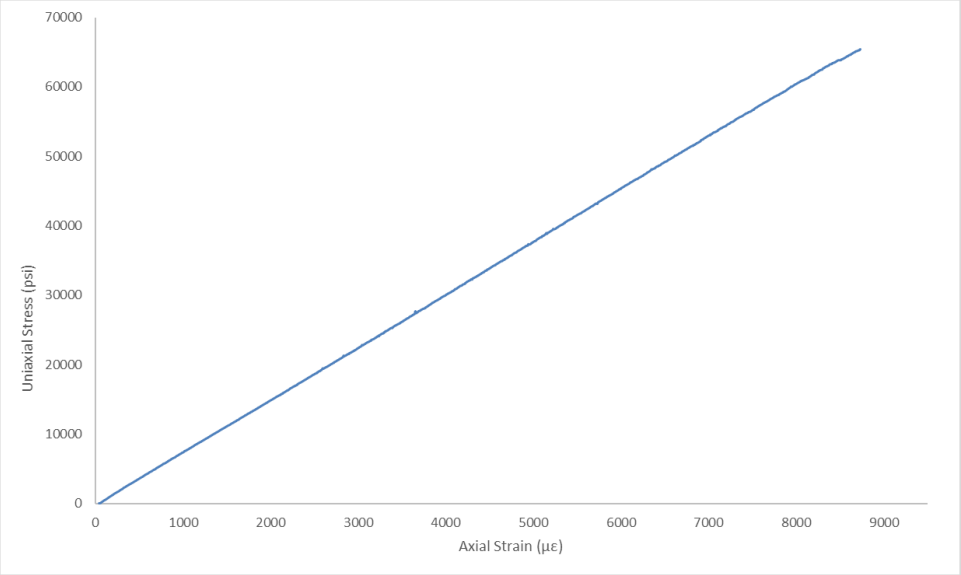

Figure 15. Plot of Uniaxial Stress vs Axial Strain to determine the Laminate Failure Strength

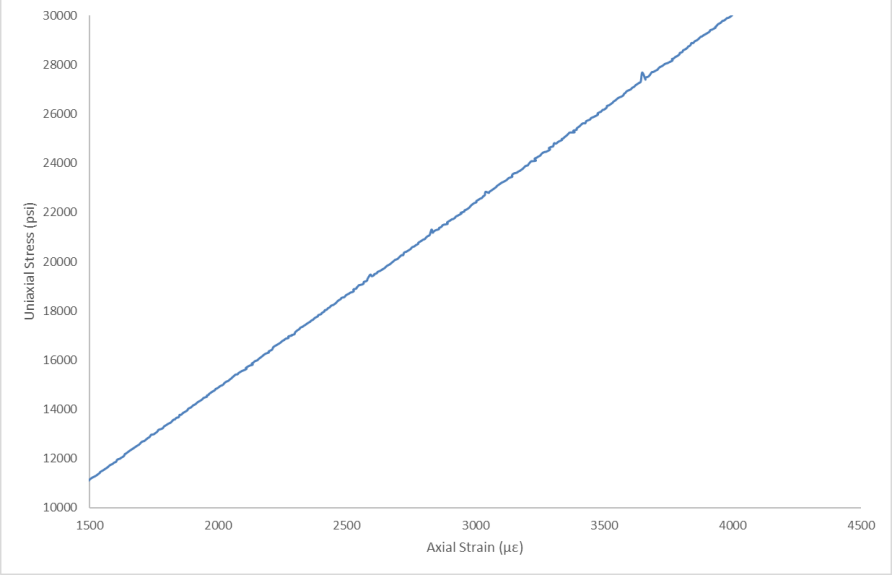

Figure 16. Plot of Uniaxial Stress vs Axial Strain zoom in on the Chord Modulus Measurement

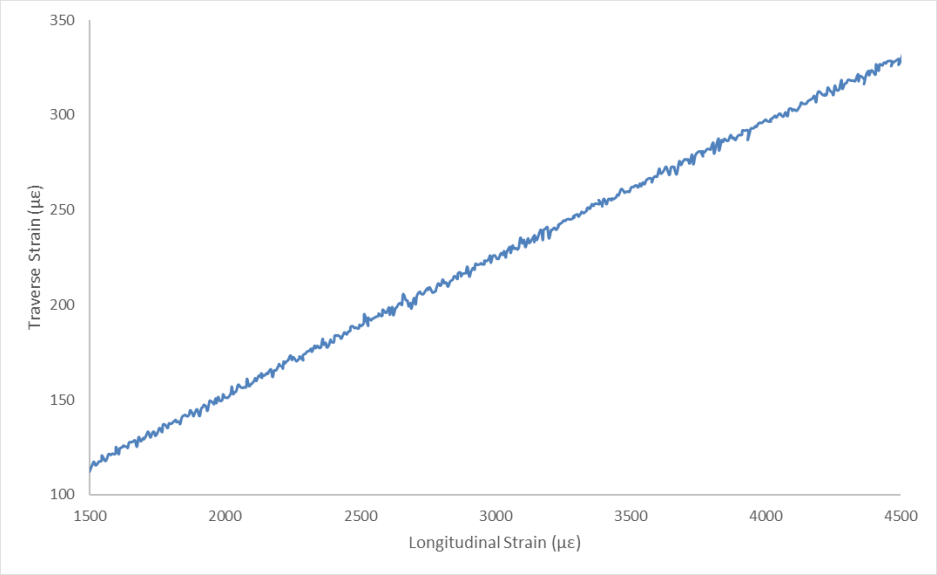

Figure 17. Plot of Negative Traverse Strain vs Longitudinal Strain zoom in on Chord Method for Poisson's Ratio

The examination of tensile properties for materials oriented at [0°/90°], as guided by the ASTM standard D3039/D3039M, provides evidence of their mechanical behavior. The analysis, supported by Figure 15, identifies the material's response to stress as purely elastic. In table 5, Modulus of Elasticity (E) of 7.6 KSI, using the chord method on Figure 16 (see Appendix for detailed methodology), highlights the material's stiffness, a critical measure of its resistance to deformation under applied load. Additionally, the Poisson's Ratio at 0.0720 calculated using the chord method on Figure 17, offers insight into the material's dimensional change in the lateral direction when subjected to longitudinal stress, indicating a moderate tendency for lateral expansion. The Ultimate Tensile Strength (F^{tu}), captured at 65.437 ksi, along with an Ultimate Tensile Strain of 8730 με, as depicted in Figure 15, underlines the material's robustness, illustrating its ability to withstand substantial deformation prior to failure. Based of the Precision Statistics table in D3039/D3039M, the values calculated using the data recorded by strain gages are around the values given the table. These findings not only outline the material's elastic behavior but also its significant capacity for enduring stress, providing an understanding of its mechanical properties in response to tensile forces.

Table 5. In-plane tensile material properties for $[0°/90°]_s$ per ASTM standard D3039/D3039M.				
Modulus, E (by chord method)	Poisson's Ratio, (by chord method)	Maximum Force, P^{max}	Ultimate Tensile Strength, F^{tu}	Ultimate Tensile Strain,
7.6 ksi	0.0720	6030 lb	65.437 ksi	8730 με

The findings from this experiment involve how different orientations of fibers within composite materials change their mechanical responses to stress and strain. At failure, these specimens behaved differently and showed different signs of failure. The [+45°/-45°] orientation specimen broke diagonally, as shown in

Appendix Figure 22 and 21, whereas the [0°/90°] orientation broke horizontally. This again is due to the orientation of the fiber of the specimen.

Through the data collected using strain gages and subsequent stress-strain analysis, we observed that the orientation of fibers plays a crucial role in dictating the material's strength and resilience. The [+45°/-45°] orientation exhibited enhanced shear properties, whereas [0°/90°] orientation demonstrated enhanced tensile properties. This outcome suggests that the alignment of fibers can be strategically manipulated to get the most out of mechanical properties of composite materials for specific engineering applications.

It becomes evident that the structural arrangement of fibers within a composite material is not merely a matter of physical assembly but a critical factor in engineering the material's response to external forces. The superior performance of the [+45°/-45°] orientation aligns with theoretical predictions about anisotropic behavior in composite materials, where directional dependence on properties is expected. This finding not only validates the initial hypothesis that fiber orientation significantly impacts material properties but also opens up avenues for further research. Moreover, the methodology applied in this experiment, leveraging precise strain measurements, sets a robust framework for quantitatively assessing the influence of structural variables on material performance.

Conclusion:

The comprehensive analysis of the experiment's results underscores the pivotal role of fiber orientation in enhancing the mechanical properties of composite materials. The comparison between the two specimens, [0°/90°] fiber orientation and [+45°/-45°] orientation, illustrates a significant difference in their response to applied stresses. The specimen with the [+45°/-45°] orientation demonstrated superior shear properties while the [0°/+90°] orientation demonstrated superior tensile properties which substantiates the initial hypothesis that the arrangement of fibers can dramatically influence a material's strength and durability. This observation aligns with established theories, confirming the consistency of the experimental findings with the expected outcomes. The use of strain gages for precise measurements further validates the experiment's methodology and outcomes, providing a reliable assessment of fiber orientation's effect on material properties.

These findings will help future research and application in choosing orientation of fibers within composite materials which can be used for their mechanical properties. The properties observed in the [+45°/-45°] and [0°/90°] specimens can be used in different fields of Engineering and for specific applications. Moreover, the consistency of the experimental results with theoretical predictions provides a solid foundation for developing predictive models to forecast the behavior of materials under various stress conditions.

Applications:

In the realm of aerospace engineering, strain gages find extensive use across a diverse array of applications, including load testing of different aircraft components during structural integrity assessments, monitoring the performance of aircraft components in wind tunnel testing, and testing the mechanical behavior of composite materials before they make their way into aircraft designs. These examples are not the extensive list of applications for aerospace engineering, in fact they are barley the tip

of the iceberg. Despite the wide-ranging nature of these applications, the underlying principles and methodologies for stress and strain analysis of materials using strain gauges remain unwavering.

The specific application that will be discussed in this section is based on an article titled *Structural Testing of a Shear Web Attachment Point on a Composite Lattice Cylinder for Aerospace Applications* [9]. This article details a study in which a 1.5-meter diameter lattice satellite central cylinder underwent experimental testing and numerical analysis utilizing strain gages, linear variable differential transformers, and a digital image correlation system. The goal behind this study was to prove the effectiveness of the lattice cylinder compared to a traditional cylinder for similar aerospace applications.

The lattice cylinder studied was comprised of Toray Advanced Composites RS-36/M55J Uniaxial prepreg which is an ideal material for space applications due to the low outgassing properties and sound mechanical properties. Specifically, a laminate patch was placed on the external circumference of the lattice cylinder which was 16 plies thick and featured a quasi-isotropic configuration comprised of 0-, 90-, 45-, and -45-degree layers. Strain gages were implemented on both the internal and external surface of the lattice cylinder on both the ribs of the cylinder and laminate patch to gather data. The specific strain gages used were not listed, however they consisted of a compliant rod element connecting to nodes which defined a positive and negative end of the gage [9].

Strain results were gathered from load cell readings at 4000N, 5500N, and 6500N with loads applied in increments of 1000N per 60 seconds. The readings were then compared with the predicted results which were gathered in a finite element computer simulated model. The article concluded that almost all strain results agreed within a ±20% deviation band for both the simulated and physical tests at the three different maximum loads. The results further demonstrate the advantages of the lattice cylinder, specifically within the realms of reduction in mass, reduced manufacturing cost, reduced lead time, and improved accessibility with an open structure [9].

In this study, 24 strain gauges were simultaneously employed to gather comprehensive data on a large structure, strategically configured to minimize tooling efforts while effectively capturing global structural behavior [9]. Such utilization underscores the remarkable versatility of strain gauges within engineering applications, showcasing their adaptability across various fields of study. The findings not only affirm the efficacy of strain gauges in providing valuable insights into structural dynamics but also highlight their capacity to streamline testing processes and enhance overall efficiency. This study underscores the enduring relevance and utility of strain gauges as indispensable tools in engineering research and practice.

References:

[1] R. Hamilton. “Summarizing Elementary Theory of Elasticity” *Pennsylvania State University (2024)* https://psu.instructure.com/courses/2310697/assignments/syllabus

[2] R. Hamilton. “Electrical Resistance Strain Gages Part 1: Principles of Operation” *Pennsylvania State University (2024)* https://psu.instructure.com/courses/2310697/assignments/syllabus

[3] R. Hamilton. “Electrical Resistance Strain Gages Part 2: Principles of Operation” *Pennsylvania State University (2024)* https://psu.instructure.com/courses/2310697/assignments/syllabus

[4] R. Hamilton. “Strain gage Circuits and Instrumentation 1” *Pennsylvania State University (2024)* https://psu.instructure.com/courses/2310697/assignments/syllabus

[5] R. Hamilton. “Lab 1 Part 1: Installing Electrical Resistance Strain Gages” *Pennsylvania State University* (2024) https://psu.instructure.com/courses/2310697/pages/lab-1-part-1-installing-electrical-resistance-strain-gages?module_item_id=41001548

[6] *VARTM*. The Gund Company. (2023, August 24). https://thegundcompany.com/capabilities/materials-manufacturing/vartm/

[7] *Key strain gage terms and definitions*. Micro. (n.d.). https://www.micro-measurements.com/resources/definitions

[8] R. Hamilton. “Lab 1 Part 2: Data Analysis: Mechanical Behavior and In-Plan Material Properties” *Pennsylvania State University* (2024) https://psu.instructure.com/courses/2310697/pages/lab-1-part-2-data-analysis-mechanical-behavior-and-in-plane-material-properties?module_item_id=41001555

[9] Smeets, B. J. R., Fagan, E. M., Matthews, K., Telford, R., Murray, B. R., Pavlov, L., Weafer, B., Meier, P., & Goggins, J. (2021). Structural testing of a shear web attachment point on a composite lattice cylinder for aerospace applications. *Composites Part B: Engineering*, *212*, 108691. https://doi.org/10.1016/j.compositesb.2021.108691

Appendix:

(a)

(b)

Figure 18. Strain Gage Specifications: **(a)** Illustrating the manufacturer specifications on the front; and (b) back of the CEA-00-375UW-120 strain gage packaging.

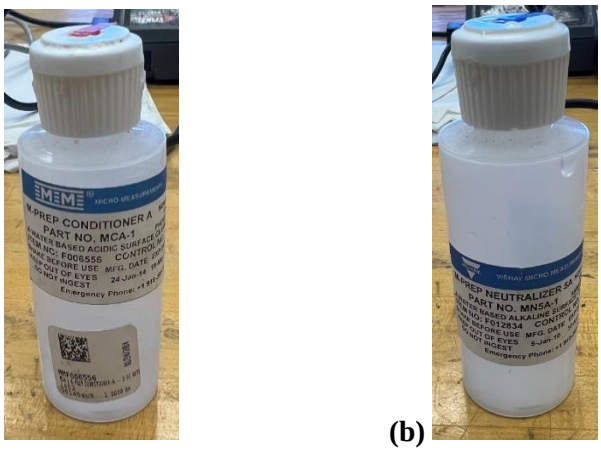

Figure 19. Strain Gage Preparation Supplies: (a) M-prep conditioner A bottle; and (b) M-prep neutralizer 5A bottle

Figure 20. Well Bonded Un-Soldered Strain Gages: Visually demonstrates strain gages bonded correctly in the transverse and axial direction after tape removal.

Figure 21, [0°/90°] Specimen after failure

Figure 22. [+45°/-45°] Specimen after failure

Chord Shear Modulus of Elasticity

$$G_{12}^{chord} = \frac{\Delta\tau_{12}}{\Delta\gamma_{12}}$$

Where

G^{chord} = Shear chord modulus of elasticity

$\Delta\tau_{12}$= difference in applied shear stress

$\Delta\gamma_{12}$= difference between the two shear strain points.

Tensile Chord Modulus of Elasticity

$$E^{chord} = \frac{\Delta\sigma}{\Delta\varepsilon}$$

Where

E^{chord} = tensile chord modulus of elasticity

$\Delta\sigma$ = difference in applied tensile stress between the two strain points

$\Delta\varepsilon$ = difference between the two strain points

Poisson's Ratio by Chord Method

$$\nu = -\frac{\Delta\varepsilon_t}{\Delta\varepsilon_l}$$

Where

ν = Poisson's Ratio

$\Delta\varepsilon_t$ = difference in lateral/traverse strain between the two longitudinal strain points

$\Delta\varepsilon_l$ = difference between the two longitudinal strain points

Maximum Shear Stress

$$\tau_{12}^{m} = \frac{P^m}{2A}$$

Where

τ_{12}^{m} = maximum in-plane shear stress

P^m = Maximum load at or below 5% shear strain

A= cross-sectional area in accordance with Test method D3039/D 3039M

Ultimate Tensile Strength

$$F^{tu} = \frac{P^{max}}{A}$$

Where

F^{tu} = Ultimate Tensile Strength

P^{max} = maximum force before failure

A = Average cross-sectional area